You may also be interested in:

Instantons in a Lagrangian model of turbulence

L S Grigorio[1,2]**, F Bouchet**[1]**, R M Pereira**[1,3] **and L Chevillard**[1]

[1] Univ. Lyon, École Normale Supérieure de Lyon, Univ. Claude Bernard, CNRS, Laboratoire de Physique, F-69342 Lyon, France
[2] Centro Federal de Educação Tecnológica Celso Suckow da Fonseca, Av. Governador Roberto Silveira 1900, Nova Friburgo, 28635-000, Brazil
[3] Mechanical Engineering Program, Federal University of Rio de Janeiro (COPPE/UFRJ), Rio de Janeiro, 21941-594, Brazil

E-mail: leonardo.grigorio@cefet-rj.br

Abstract

The role of instantons is investigated in the Lagrangian model for the velocity gradient evolution known as the recent fluid deformation approximation. After recasting the model into the path-integral formalism, the probability distribution function (pdf) is computed along with the most probable path in the weak noise limit through the saddle-point approximation. Evaluation of the instanton solution is implemented numerically by means of the iteratively Chernykh–Stepanov method. In the case of the longitudinal velocity gradient statistics, due to symmetry reasons, the number of degrees of freedom can be reduced to one, allowing the pdf to be evaluated analytically as well, thereby enabling a prediction of the scaling of the moments as a function of Reynolds number. It is also shown that the instanton solution lies in the Vieillefosse line concerning the RQ-plane. We illustrate how instantons can be unveiled in the stochastic dynamics performing a conditional statistics.

Keywords: instantons, large deviation, Lagrangian turbulence

(Some figures may appear in colour only in the online journal)

1. Introduction

This paper aims at obtaining the stationary probability distribution function and large fluctuations of a stochastic model of turbulence proposed by Chevillard and Meneveau [1]. The model, known as recent fluid deformation (RFD) approximation, consists in a set of stochastic differential equations describing the evolution of the eight degrees of freedom of the velocity gradient tensor of a fluid particle along its Lagrangian trajectory in an incompressible flow.

Large deviations of the velocity gradient in turbulent flows are associated with high dissipation rates and enstrophy and are crucial to the understanding of intermittency phenomena—a topic of intense research in turbulence. In order to evaluate the probability distribution functions (pdfs) of the velocity gradients (and also the probability of large fluctuations) we make use of the iterative numerical procedure of Chernykh–Stepanov [2] which amounts to solving the saddle-point equations that minimize the action. This method provides the most probable path leading to a given fluctuation, which will be referred to as the instanton. In the case of the longitudinal velocity gradient, the number of degrees of freedom can be reduced to one, due to symmetry, allowing the pdf to be obtained analytically as well. These analytically obtained pdfs are in excellent agreement with the numerical ones obtained by numerical integration of the stochastic differential equations. Another result is that the instanton lies along the Vieillefosse line in the so-called *RQ*-plane. For the longitudinal velocity gradient, this instanton approach gives unprecedented prediction for the pdf tail and for the dynamics of the optimal path, along with a prediction of how the moments scale with the Reynolds number. That gives us a theoretical approach to the dynamics leading to these rare events, and thus intermittency. This point is the main originality of this work.

Of central interest in the area of turbulence is the behavior of small scale statistics. More specifically, scaling and universality at small scales of motion in turbulent flows is a long standing problem [3]. Due to the intense fluctuations within small scales, large deviations of velocity field differences are very pronounced for high values of Reynolds number. These large excursions of the velocity gradient are apparent in the pdf, where drastic departures from Gaussian behavior are manifest—and also termed intermittency.

It is clear that a theory of turbulence capable of explaining intermittency and the scaling of high order structure functions must rely on a deep understanding of the dynamics of the small scales. A natural candidate to probe such scales is the velocity gradient tensor. Nevertheless, obtaining the statistics of the velocity gradient tensor is a difficult task. A common approach to address the evolution of the velocity gradient is the Lagrangian framework, which can drastically reduce the degrees of freedom and lead to a simplified picture of the small scales. Turbulence in the Lagrangian frame has some different features to Eulerian turbulence, such as a shorter correlation time of the velocity gradient. This property inspired the recent fluid deformation [1] approximation, which is a model where the shape of a fluid particle following the local velocity field has a short memory. This closure was studied in the last years [4–6] and extended to account for passive scalar transport and MHD [7] and was dealt with analytically by an effective action approach, based on noise renormalisation [8].

In order to study large deviations of the velocity gradients in this model the path integral framework is used, which is particularly suitable to investigate large fluctuations. The reason lies in the fact that for weak noise driven systems, the probability is dominated by the action minima. The trajectory which minimizes the action is called instanton. This approach is equivalent to the Freidlin–Wentzell theory of large fluctuations [10] and provides a proper way to find which is the most probable evolution leading to a large event. It can be, therefore, a valuable approach to deal with an important question in hydrodynamic turbulence, that is, what are the common structures found at small scale turbulence? Structures related to large values of velocity gradient are of vital importance in the study of turbulence, since they are responsible for most of dissipation that takes place at the smallest scales of fluid motion, typically associated with large strain and vorticity. Many works have devoted significant effort to the identification of such objects. In particular the use of instanton techniques to achieve this goal in Burgers turbulence can be found in [2, 19–21]. Moriconi *et al* [8] applied the path-integral approach to evaluate the pdf in the RFD model. However, the set of saddle-point

equations was linearized to obtain an approximate instanton solution. To correct this truncated saddle-point equations, a perturbative method was carried out.

In this work we determine the instanton of the RFD, addressing the question of what is the most probable evolution of a Lagrangian particle and also calculating its contribution to the pdf in the weak noise limit by solving the full set of non-linear saddle-point equations. For the case of a diagonal (longitudinal) component of the velocity gradient, the analytical results can be computed for its pdf.

The paper is organized as follows. In section 2 the recent fluid deformation equations are reviewed. Section 3 is devoted to the results and is divided into four parts. Part A presents the model addressed in the Martin–Siggia–Rose/Janssen/de Dominicis path integral formalism [15–17] and how this approach can be used to address large deviations. Part B displays the transverse velocity gradient statistics after solving the instanton equations by means of the numerical Chernykh–Stepanov [2] algorithm. In part C it is shown that the longitudinal velocity gradient is subject to an analytical solution in addition to the numerical one. In the sequel, part D presents how instantons are uncovered by performing conditioned statistics with respect to the stochastic dynamics, which are confronted with the previously obtained instantons. Final remarks close the paper in section 4.

2. The RFD Lagrangian stochastic model

2.1. Recent fluid deformation for Lagrangian turbulence

Proposed in [1], the RFD is a scheme for modelling the evolution of velocity gradient of a fluid particle along its trajectory in the Lagrangian frame. By taking the gradient of the Navier–Stokes equation, we write

$$\frac{\mathrm{d}A_{ij}}{\mathrm{d}t} = -A_{ik}A_{kj} - \frac{\partial^2 p}{\partial x_i \partial x_j} + \nu \frac{\partial^2 A_{ij}}{\partial x_m \partial x_m}, \tag{2.1}$$

where $\mathrm{d}/\mathrm{d}t$ is the convective derivative, p stands for pressure divided by fluid density and ν corresponds to the kinematical viscosity. In equation (2.1), $A_{ij} = \partial_j u_i$ is the velocity gradient tensor in cartesian components. The difficulty in obtaining statistics from the velocity gradient Navier–Stokes is that the pressure Hessian and the viscous term are not closed in terms of a Lagrangian trajectory. A review of different attempts of closures can be found at [9]. The simplest closure is achieved by neglecting dissipation and nonlocal effects of the pressure Hessian. Although, a solution is available, it can be shown that it develops a divergence at finite time [12, 13]. The RFD has the merit of incorporating pressure and viscous effects preventing divergences in $\mathbb{A}$. It may be compared to the tetrad model [14], though instead of dealing with an equation for the evolution of fluid deformation, it is strongly modelled. The rationale goes as follows. Write the pressure Hessian as

$$\frac{\partial^2 p}{\partial x_i \partial x_j} \approx \frac{\partial X_m}{\partial x_i} \frac{\partial X_n}{\partial x_j} \frac{\partial^2 p}{\partial X_m \partial X_n} \tag{2.2}$$

where $\partial X_j / \partial x_i$ denotes the Jacobian of the change of coordinates from Eulerian to Lagrangian coordinates. In (2.2), spatial derivatives of the Jacobian were neglected. The Cauchy–Green tensor, defined by

$$C_{ij} = \frac{\partial x_i}{\partial X_k} \frac{\partial x_j}{\partial X_k} \tag{2.3}$$

is assumed to have the form

$$\mathbb{C} = \exp[\tau\mathbb{A}]\exp[\tau\mathbb{A}^{\mathrm{T}}], \tag{2.4}$$

where τ corresponds to a short time associated to the correlation time of the velocity gradient in the Lagrangian frame, assumed to be of the order of the Kolmogorov time scale. The idea behind the RFD approximation is that after a short period of time ($\sim \tau$) the shape of a Lagrangian particle is uncorrelated with its initial shape. Therefore, it is possible to assume an isotropic shape for a fluid particle at initial time, which implies an isotropic pressure Hessian $\frac{\partial^2 p}{\partial X_m \partial X_n} = \frac{1}{3}\delta_{mn}\frac{\partial^2 p}{\partial X_l \partial X_l}$. Taking this into account, (2.2) turns to

$$\frac{\partial^2 p}{\partial x_i \partial x_j} \approx \frac{C_{ij}^{-1}}{C_{qq}^{-1}} A_{mn} A_{nm}. \tag{2.5}$$

Similar reasoning can be applied to model the viscous term, yielding

$$\nu \frac{\partial^2 A_{ij}}{\partial x_m \partial x_m} \approx \frac{\partial X_k}{\partial x_m}\frac{\partial X_l}{\partial x_m}\frac{\partial^2 A_{ij}}{\partial X_k \partial X_l} \approx -\frac{1}{3T}C_{qq}^{-1}A_{ij} \tag{2.6}$$

where T stands for the integral time scale, which comes from dimensional arguments as $\nu/(\partial X)^2 \approx 1/T$, considering that ∂X is on the order of a typical distance travelled by a particle during time τ, which scales with the Taylor microscale length. Therefore, substituting equations (2.5) and (2.6) in (2.1), the RFD model equation is given by

$$\dot{\mathbb{A}} = \quad \mathbb{V}(\mathbb{A}) + g\mathbb{F}, \quad \text{with}$$
$$\mathbb{V}(\mathbb{A}) = -\mathbb{A}^2 + \frac{\mathbb{C}^{-1}\mathrm{Tr}(\mathbb{A}^2)}{\mathrm{Tr}(\mathbb{C}^{-1})} - \frac{\mathrm{Tr}(\mathbb{C}^{-1})}{3T}\mathbb{A}. \tag{2.7}$$

A random force $\mathbb{F}$ was supplemented to the model equation (2.7) to provide stationary statistics. In (2.7), g is the strength of the stochastic force, related to energy injection rate, and will play an important role in the discussion. $\mathbb{F}$ is a zero average white noise tensor such that

$$\langle F_{ij}(t)F_{kl}(t')\rangle = G_{ijkl}\delta(t - t'), \tag{2.8}$$

with

$$G_{ijkl} = 2\delta_{ik}\delta_{jl} - \frac{1}{2}\delta_{il}\delta_{jk} - \frac{1}{2}\delta_{ij}\delta_{kl}. \tag{2.9}$$

The force correlator G_{ijkl} is the general 4th-order tensor which respects isotropy and also ensures incompressibility, i.e. $\mathrm{Tr}\,\mathbb{A} = 0$. It can be shown that $G_{jjkl} = 0$ and $G_{ijkl} = G_{klij}$, which follow immediately from equation (2.8).

Throughout the paper all calculations will be carried out with $\mathbb{V}(\mathbb{A})$ truncated at order $\mathcal{O}(\tau^2)$ [8], hence

$$\mathbb{V}(\mathbb{A}) = \sum_{p=1}^{4}\mathbb{V}^{(p)}(\mathbb{A}), \tag{2.10}$$

$$V^{(1)}(\mathbb{A}) = -\mathbb{A}, \tag{2.11}$$

$$V^{(2)}(\mathbb{A}) = -\mathbb{A}^2 + \frac{\mathbb{I}}{3}\mathrm{Tr}(\mathbb{A}^2) + \frac{2\tau}{3}\mathrm{Tr}(\mathbb{A})\mathbb{A}, \tag{2.12}$$

$$V^{(3)}(\mathbb{A}) = -\frac{\tau}{3}\left(\mathbb{A} + \mathbb{A}^{\mathrm{T}} - \frac{2\mathbb{I}}{3}\mathrm{Tr}(\mathbb{A})\right)\mathrm{Tr}(\mathbb{A}^2) - \frac{\tau^2}{3}\mathrm{Tr}(\mathbb{A}^{\mathrm{T}}\mathbb{A})\mathbb{A} - \frac{\tau^2}{3}\mathrm{Tr}(\mathbb{A}^2)\mathbb{A}, \tag{2.13}$$

$$V^{(4)}(\mathbb{A}) = -\frac{\mathbb{I}}{9}\tau^2\mathrm{Tr}(\mathbb{A}^{\mathrm{T}}\mathbb{A})\mathrm{Tr}(\mathbb{A}^2) - \frac{\mathbb{I}}{9}\tau^2[\mathrm{Tr}(\mathbb{A}^2)]^2 + \frac{4\mathbb{I}}{27}\tau^2[\mathrm{Tr}(\mathbb{A})]^2\mathrm{Tr}(\mathbb{A}^2)$$

$$+ \frac{\tau^2}{3}\mathbb{A}^{\mathrm{T}}\mathbb{A}\,\mathrm{Tr}(\mathbb{A}^2) + \frac{\tau^2}{6}(\mathbb{A}^2 + (\mathbb{A}^{\mathrm{T}})^2)\mathrm{Tr}(\mathbb{A}^2). \tag{2.14}$$

The model possesses two non-dimensional parameters, τ/T which scales as $\mathrm{Re}^{-1/2}$ and $g/T^{3/2}$. Without loss of generality, time units can be chosen to set T equal to 1. We continue to call these parameters τ and g by abuse of notation in the remainder of the paper. All numerics have been performed with $\tau = 0.1$, which corresponds to a low Reynolds number regime.

3. Results

3.1. Instantons in the Martin–Siggia–Rose path integral

As in many applications of large deviations, it is customary to evaluate the probability to reach a final state $\mathbb{A}(t_2) = \mathbb{A}_2$ at time $t = t_2$ starting from time t_1, with $\mathbb{A}(t_1) = \mathbb{A}_1$. The initial configuration $\mathbb{A}_1$ is usually taken to be at, or close to, an attractor of the deterministic dynamics, whilst the initial time is assumed to be $t_1 = -\infty$, such that the stationary transition probability will depend solely on $\mathbb{A}(t_2)$. In this work, we want to evaluate the probability of finding a large value of one component $A_{\alpha\beta}(t_2)$, either longitudinal, or transverse, which can be accomplished with the auxiliary of the Martin–Siggia–Rose/Janssen/de Dominicis path integral [15–17]. We are interested in the case when a large velocity gradient $A_{\alpha\beta}$ occurs, so it is convenient to evaluate the following generating functional

$$\mathbb{E}[\exp[\lambda A_{\alpha\beta}(t_2)/g^2]] = \int D[\mathbb{A}]D[\hat{\mathbb{A}}] \exp\left[-S_{\mathrm{MSR}}[\mathbb{A}(t), \hat{\mathbb{A}}(t)]\right] \mathrm{e}^{\lambda A_{\alpha\beta}(t_2)/g^2}, \tag{3.1}$$

with the Martin–Siggia–Rose action,

$$S_{\mathrm{MSR}}[\mathbb{A}, \hat{\mathbb{A}}] = \int_{t_1}^{t_2}\left[\frac{g^2}{2}\hat{A}_{ij}G_{ijkl}\hat{A}_{kl} - \mathrm{i}\,\mathrm{Tr}[\hat{\mathbb{A}}^{\mathrm{T}}(\dot{\mathbb{A}} - \mathbb{V}(\mathbb{A}))]\right], \tag{3.2}$$

By rescaling the auxiliary variable $\hat{\mathbb{A}} \to \hat{\mathbb{A}}' = g^2\hat{\mathbb{A}}$ the action changes as $S_{\mathrm{MSR}}[\mathbb{A}, \hat{\mathbb{A}}] \to \tilde{S}_{\mathrm{MSR}}[\mathbb{A}, \hat{\mathbb{A}}']/g^2$.

For small g, the sum over all paths in the above equation is dominated by the action minima, so that it can approximated by

$$\mathbb{E}[\exp[\lambda A_{\alpha\beta}(t_2)/g^2]] \approx \mathrm{e}^{-g^{-2}(\tilde{S}_{\mathrm{MSR}}[\mathbb{A}^*, \hat{\mathbb{A}}'^*] - \lambda A^*_{\alpha\beta}(t_2))}, \tag{3.3}$$

where $\mathbb{A}^*$ and $\hat{\mathbb{A}}'^*$ stand for the minimizers of the action supplemented by the term $\lambda A^*_{\alpha\beta}(t_2)/g^2$. The usefulness of this functional is made clear by the large deviation theory [10]. Owing to the Varadhan's theorem [11] if $A_{\alpha\beta}$ obeys a large deviation principle with rate function $S(a) = -g^2\ln\rho_{\alpha\beta}(a)$, where $\rho_{\alpha\beta}(a)$ is the probability to find $A_{\alpha\beta}(t_2) = a$ starting from $\mathbb{A}(t_1 = -\infty) = 0$, the so-called scaled cumulant generating functional

$$G(\lambda) = g^2\ln\mathbb{E}[\exp[\lambda A_{\alpha\beta}(t_2)/g^2]] \tag{3.4}$$

may be expressed for large λ/g^2 as

$$
\begin{aligned}
G(\lambda) &= g^2 \ln \left[\int \mathrm{d}a \ \mathrm{e}^{g^{-2}S(a)} \mathrm{e}^{g^{-2}\lambda a} \right] \\
&\approx g^2 \ln \left[\mathrm{e}^{(-g^{-2}) \min_a \{S(a) - \lambda a\}} \right],
\end{aligned}
\tag{3.5}
$$

where the integration was carried out by the Laplace method. As a consequence $G(\lambda)$ and $S(a)$ are related by a Legendre–Fenchel transform

$$
G(\lambda) = - \min_a \{S(a) - \lambda a\},
\tag{3.6}
$$

with $\lambda = \partial S/\partial a$. By comparing (3.3) and (3.6) one can identify the rate function with the action minima. After substituting $-i\hat{\mathbb{A}}(t)$ by $\mathbb{P}(t)$ in (3.2), the action minimization leads to

$$
\dot{A}_{ij} = V_{ij}(\mathbb{A}) + g^2 G_{ijkl} P_{kl}
\tag{3.7}
$$

$$
\dot{P}_{ij} = -P_{kl} \nabla_{ij} V_{kl}(\mathbb{A}),
\tag{3.8}
$$

subject to boundary conditions $P_{ij}(t_2 = 0) = -\lambda \, \delta_{i\alpha}\delta_{j\beta}$ and $A_{\alpha\beta}(t_1 = -\infty) = 0$.

We refer the reader to the appendix where it is shown how the term $\lambda A_{\alpha\beta}(t_2)$ implies a final condition for the auxiliary variable $\mathbb{P}$. The set of mixed initial–final condition equations (3.7) and (3.8) naturally suggests that $\mathbb{P}$ should be integrated backwards in time whereas $\mathbb{A}$ is integrated forwards in time. This kind of problem was tackled numerically by Chernyk and Stepanov [2] and by [20, 21] in the context of the Burgers equation, where they were interested in how strong values of the velocity gradient develop. It was found that instantons were shock-like, which are known to play an important role in the underlying dynamics of the system. See also [22] for a review of applications of this approach, including the study of instantons in the stochastic Navier–Stokes equation.

For the sake of clarity, we split the cases where the fixed final value of the velocity gradient is either one of the diagonal (longitudinal) or off-diagonal (transverse) components.

3.2. Transverse gradient statistics

This section shows the results regarding the stationary statistics $\rho_{12}(a)$ of the transverse velocity gradient. Due to numerical reasons we should use a finite but large initial time t_1. In our implementation we chose $t_1 = -6T$ whereas $t_2 = 0$, that is, the evolution is carried out through six integral time scales. It was also checked numerically that this value suffices for stationarity by examining the time series of the original SDE, integrated according to [24]. The algorithm is an iterative procedure to obtain the solution of the set of equations (3.7) and (3.8).

Before we apply the method treating the eight independent degrees of freedom encoded in $\mathbb{A}$, it is convenient to take advantage of the symmetries of the problem in order to reduce the number of degrees of freedom, lowering thus the computational cost. First, recall the functional (3.1). The lambda term can be understood as another term in the action of the form $\lambda\delta(t - t_2) A_{\alpha\beta}(t)$ (in this section $(\alpha, \beta) = (1, 2)$). This additional term, which manifests itself in the equations of motion (3.7) and (3.8) as a final condition for $\mathbb{P}$, breaks the parity symmetry $x_i \to -x_i$ and $v_i \to -v_i$ for $i = 1,2$, therefore only the symmetry $x_3 \to -x_3$ and $v_3 \to -v_3$ remains. If the action exhibits this symmetry so does the solution to the equations of motion, provided the final/initial conditions keep the same symmetry, which is the case. Hence $\mathbb{A}$ must be a velocity gradient tensor with reflection symmetry in the x_3 direction, whose only possible form is
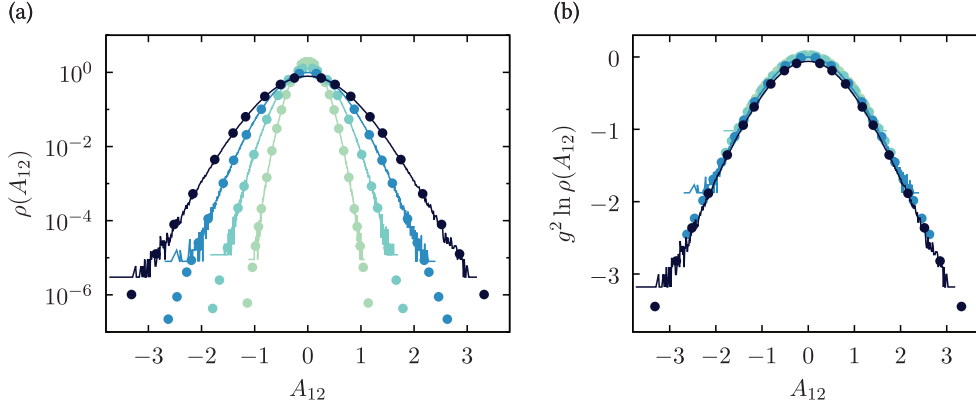
Figure 1. (a) Semilog plot of the transverse velocity gradient pdf. Dots: numerical instanton evaluation. Solid lines: pdfs from SDE (2.7). The range of A_{12} lies between five and six standard deviations. The forcing values are $g = 0.2, 0.3, 0.4$ and 0.5, where darker colours correspond to higher values of g. (b) Rescaled pdfs corresponding to vertical axis $g^2 \ln \rho(a)$ showing collapse.

$$
\mathbb{A}(t) = \begin{pmatrix} A_{11}(t) & A_{12}(t) & 0 \\ A_{21}(t) & A_{22}(t) & 0 \\ 0 & 0 & -A_{11}(t) - A_{22}(t) \end{pmatrix}.
\tag{3.9}
$$

We are left with four independent variables instead of eight, which simplifies the computation considerably.

Now, the Chernyk–Stepanov method can be performed. The idea is to decouple $\mathbb{P}(t)$ and $\mathbb{A}(t)$ for the first iteration. For instance, we set $\mathbb{A}(t) = 0$ and solve (3.8) backwards in time for an arbitrarily chosen λ. In the next step, we substitute the time series of $\mathbb{P}(t)$ obtained in (3.7), which is integrated forward in time to obtain $\mathbb{A}(t)$. This is performed recursively until the solutions converge. Both equations are solved by the 4th order Runge–Kutta scheme with time step $dt = 10^{-3}$ and a piecewise cubic interpolation is performed to obtain the intermediate time steps required by the method. The criteria used for convergence is that $|A_{12}(0) - A_{12}^{old}(0)|/|A_{12}^{old}(0)| < \delta$, i.e. the relative error of the obtained instanton in comparison with the (old) instanton calculated in the previous iteration should be smaller than a quantity δ (we set $\delta = 10^{-7}$ and $\delta = 10^{-10}$ for the longitudinal case). With the instanton solution, the probability of arriving at a final value $A_{12} = a$ is determined by $\rho_{12}(a) \approx e^{-S(a)/g^2}$. Spanning a set o λ's we can generate the pdf $\rho_{12}(a)$, since each value of λ leads to a different final value of the longitudinal velocity gradient a. Figure 1(a) displays pdfs obtained by this approach for different values of forcing amplitude. Pdfs from numerical integration of the SDE are also plotted for comparison, showing good agreement between the results. The collapse depicted in figure 1(b) corresponds to a rescaling of the vertical axis, $g^2 \ln(\rho(A_{12}(t_2) = a))$ and shows that the pdfs calculated obey the large deviation principle. The curve is minus the rate function (action minima) as a function of the final value A_{12}.

In this paper, for simplicity we have solved the Euler–Lagrange equations using a 4th order Runge–Kutta method. The reason for this lies in fact that the instanton equations share the same form of the stochastic equations, so the numerical integration method used to solve the stochastic equations could be easily adapted to the instanton case. We have checked the

stability of the results with respect to the resolution. However, as we seek to minimize a time dependent action, by analogy to classical approaches in optimal control theory, it may have been wiser and more precise to first discretize the action, then obtain the corresponding time discrete evolution, in order to insure that the time discretized evolution equations correspond to the critical points of the discrete action. That way the discretized version of the time derivative for the auxiliary equation would have been the adjoint version of the forward equation one.

A last comment on the numerical scheme concerns the convergence issues that may arise. In fact, in the original reference of the method [2] it was reported that, for a critical value of λ, the numerical convergence becomes problematic. In our case, it is noticed that as $|\lambda|$ increases, so does the number of iterations to reach convergence. In the transverse case, where the number of degrees of freedom cannot be as reduced as in the longitudinal case (see next section), convergence may fail completely. In order to circumvent this issue we performed the following strategy. Let A^α and P^α be the α-th step in the iteration procedure of the numerical integration. The direct approach would be to use the series A^α and P^α in the saddle-point equation (3.8) to obtain $P^{\alpha+1}$ and $A^{\alpha+1}$ and so on. However, when the iteration ceases to converge, we modify $A^{\alpha+1}$ by $A^{\alpha+1} \rightarrow \beta A^\alpha + (1-\beta)A^{\alpha+1}$, with β arbitrarily chosen on the interval [0,1], that is, the next iteration is a weighted average of the old and the new ones. Although not systematic, since we do not know *a priori* which is the optimal β value, this procedure dumps large variations in each step and tends to keep iterations inside the converge radii. Values as big as $\beta = 0.8$ may be needed to capture the tail of the distributions.

3.3. Longitudinal gradient statistics

In this section we show the results concerning the longitudinal velocity gradient. In order to calculate the instanton we make use of the even higher degree of symmetry of this case, which reduces the number of degrees of freedom to only one. We invoke the same rationale of the previous section. The difference is that imposing $A_{11}(0) = a$ consequently adds to the action a term that respects parity symmetry $x_i \rightarrow -x_i$, $v_i \rightarrow -v_i$ in all directions and hence implies that the instanton velocity gradient must be diagonal. This term breaks thr rotation symmetry though, by selecting the x_1 direction, but the action is still invariant under rotations around the x_1 axis. So, the action makes no preference between the x_2 or x_3 directions, implying $A_{22} = A_{33}$ for the solution. Moreover, incompressibility leads to $\mathbb{A} = \text{diag}(A(t), -A(t)/2, -A(t)/2)$, i.e. the velocity gradient depends on a single degree of freedom. Within this simplification the saddle-point equations become much faster and stable to be integrated numerically.

Apart from the numerical solution to the saddle-point equations, the high degree of symmetry enables us to derive an analytical solution in the case of longitudinal velocity gradient. With the velocity gradient given by a diagonal form $\mathbb{A} = \text{diag}(A(t), -A(t)/2, -A(t)/2)$, a reduced MSR action for the single degree of freedom $A(t)$ can be written as

$$S_{\text{red}}[A, p] = \int_{-\infty}^{0} dt \left[p(\dot{A} - b[A]) - \frac{g^2}{2}p^2 \right], \tag{3.10}$$

where $A(t)$ is a scalar, equivalent to the A_{11} of the original system and $b[A] = V_{11}[\mathbb{A}]$. Due to this drastic reduction of degrees of freedom, it is possible to write $b[A]$ as a gradient of a function $h[a]$

$$b[A] = -\nabla h[A], \quad h[A] = \frac{A^2}{2} + \frac{A^3}{6} + \frac{\tau}{4}(1+\tau)A^4 - \frac{\tau^2}{10}A^5 + \mathcal{O}(\tau^3). \tag{3.11}$$
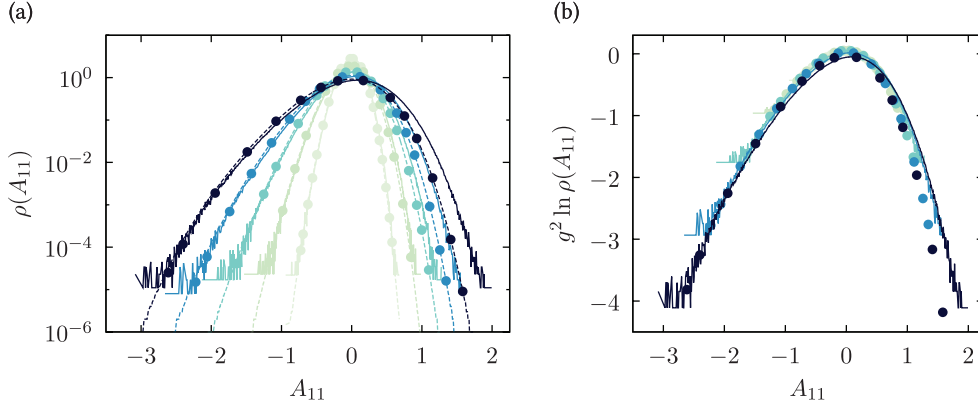
Figure 2. (a) Semilog plot of the longitudinal velocity gradient pdf. Dots: numerical instanton evaluation. Solid lines: pdfs from SDE (2.7). Dashed lines: analytical (3.13). The range of A_{11} lies between five and six standard deviations. The forcing values are $g = 0.2, 0.3, 0.4, 0.5$ and 0.6 where darker plots correspond to higher g values. (b) Rescaled pdfs corresponding to vertical axis $g^2 \ln \rho(a)$ showing collapse.

In that case, instantons may be obtained as the reverse of the relaxation path from $A(0)$ to $A(-\infty)$ [23]. Nevertheless, the pdf can be computed in a more straightforward manner by solving the corresponding Fokker–Planck equation. First, we write an effective SDE which leads to the above reduced action (3.10)

$$\dot{A} = b[A] + gf(t), \tag{3.12}$$

where $\langle f(t)f(t')\rangle = \delta(t - t')$ is the correlation of the reduced noise $f(t)$. A straightforward calculation shows that the MSR action related to the SDE (3.12) is given by (3.10). The Fokker–Planck equation can be easily derived from (3.12), whose stationary solution reads

$$\rho(a) = N \exp(-2h[a]/g^2), \tag{3.13}$$

with $h[A]$ given by (3.11) and N is normalization factor. This important result validates the numerical procedure, as one can see in figure 2(a), where a good agreement between the analytical and numerical instanton contribution to the pdf is achieved.

With respect to the domain of validity of the weak noise approximation, we expect it to be valid for $\lambda/g^2 \gg 1$ (see for instance [21]). After (3.11) and (3.13) and using $\lambda = \partial S(a)/\partial a$ we have $a \gg (g/\tau)^{1/2}$ as a condition for the instanton to be a good approximation.

Once the pdf $\rho(a)$ is obtained analytically, it is possible to evaluate the moments of the velocity gradient as a power series of the noise g along with the scaling with Reynolds number, which is another original result of this paper. A straightforward computation yields for the first central moments of the longitudinal velocity gradient,

$$\mathrm{var}[a] = \frac{g^2}{2} + \frac{g^4}{96}(29 - 180\tau(1 + \tau)), \tag{3.14}$$

$$\frac{\mathbb{E}[(a - \mathbb{E}[a])^3]}{\mathrm{var}^{3/2}[a]} = -\frac{g}{\sqrt{2}} + g^3\left(-\frac{25}{24\sqrt{2}} + \frac{15\,\tau}{\sqrt{2}} + 9\sqrt{2}\,\tau^2\right), \tag{3.15}$$
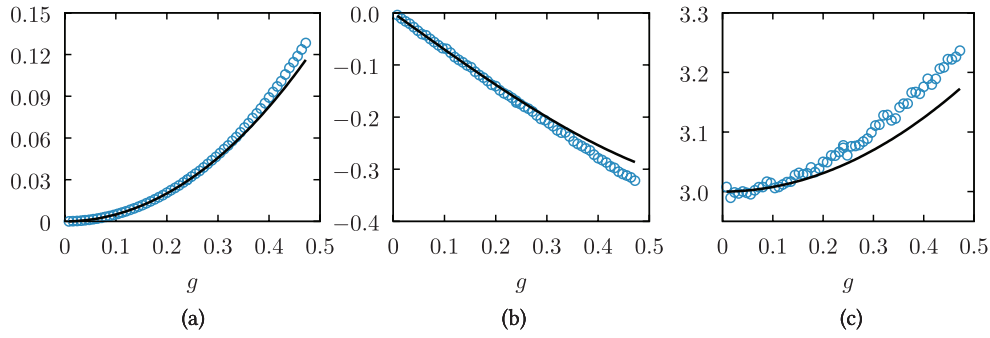
Figure 3. Statistical moments of the longitudinal velocity gradient as a function of the forcing g. Circles: numerical integration. Solid lines: instanton analytical results (equations (3.14)–(3.16)). (a) Variance. (b) Skewness. (c) Flatness.

$$\frac{\mathbb{E}[(a - \mathbb{E}[a])^4]}{\mathrm{var}^2[a]} = 3 + \frac{1}{16}g^2(19 - 60\,\tau(1 + \tau)). \tag{3.16}$$

We highlight the fact that this is a novel result specially considering there are few analytical results concerning velocity gradient models available. Let us make a connection with the phenomenology of turbulence. Equations (3.14)–(3.16) have been obtained in the asymptotic limit $g \to 0$. Equations (3.14) says that in this limit, the variance of a is given by g^2. The expected Reynolds number dependence, as predicted by Kolmogorov (i.e. $\mathrm{var}(a) \propto \mathrm{Re}$), is not reproduced here. Only at fourth order in g a Reynolds number dependence appears (through τ), which is negative and of order 1/Re as Re $\to \infty$ (if we assume that $\tau/T \propto 1/\sqrt{\mathrm{Re}}$). Thus, in this asymptotic limit $g \to 0$, the RFD closure (2.7) is not realistic for fully developed turbulent flows. When g is of order unity, numerical simulations of equation (2.7) (see for instance [25]) show indeed very different behaviors when $\tau \to 0$. Nonetheless, still in the asymptotic limit $g \to 0$, equation (3.15) shows that the RFD closure exhibits skewness for the longitudinal velocity gradient, of order g. This shows clearly that the RFD closure, and in particular the self-stretching term, can reproduce some aspects of turbulence phenomenology. In particular, this skewness of derivatives remains independent of the Reynolds number at first order in g, as expected in a non-intermittent turbulence. A slight dependence on the Reynolds number appears (of order τ^2) at third order in g. Similar interpretations can be done where flatness is concerned (equation (3.16)): in the asymptotics $g \to 0$, flatness is independent on Reynolds number and equal to three, reminiscent of non-intermittent Gaussian turbulence, and only at second order in g appears a (negative) Reynolds number dependence.

Comparison with the numerical solution of the SDE, figure 3, shows compatibility between analytical and numerical moments for small values of forcing. As g increases though, the analytical result disagrees with the numerical evaluation since for finite g the instanton approximation is not sufficient to estimate the pdf. Moreover, it can be also noted that the agreement between numerical and analytical moments decreases for higher moments, which is expected considering the analytical pdfs are a mismatch with the numerical ones in the tails (in particular the right tail), figure 2.

The skewness and flatness, though, show an incorrect scaling with respect to the Reynolds number, which points to a drawback of the model. This drawback, appearing at high Reynolds numbers, was already recognized in [25]. The new analytical results provided in equations (3.14)–(3.16) shed a new light on the numerical results obtained in [25].

Indeed, this underlined that the variance of the gradients does not behave in a consistent way with with the free parameter of the model, i.e. the Reynolds number, in line with the dimensional approach of Kolmogorov. To circumvent this issue, it was proposed instead in [25] to study the relative scaling of the logarithm of higher order moments of the gradients with respect to the variance of the gradients. To interpret the departure of the observed scalings seen in [25] from non intermittent scalings, it is then tempting to interpret them, based on the theoretical results of equations (3.14)–(3.16), as also being reminiscent of the forcing. Future works will be devoted to improve the RFD approximation in order to include genuine intermittent scalings, at the cost, perhaps, of introducing a further free parameter that quantifies in an appropriate way intermittent corrections. We leave these perspectives for future investigations.

Regarding the so-called *RQ* plane, the velocity gradient instanton starts at $\mathbb{A}_1 = 0$ evolving to a final configuration such that $A_{11}(0) = a$. If we keep track of the trajectory on the *RQ* plane it is noticed that it lies entirely in the Vieillefosse line ($4Q^3 + 27R^2 = 0$, with $Q = -\operatorname{Tr}\mathbb{A}^2/2$ and $R = -\operatorname{Tr}\mathbb{A}^3/3$) [12], although this is not a consequence of the model dynamics. Actually, this is simply due to kinematics since for a velocity gradient tensor taking the form $\mathbb{A} = \operatorname{diag}(A(t), -A(t)/2, -A(t)/2)$, which in turn is a consequence of symmetry, the Vieillefosse line is satisfied identically.

3.4. Filtering and interpretation of instanton solution

In this section we try to assess the relevance of instantons in a fluid dynamical model sharing many non-trivial properties with real turbulence, as it is the case for the RFD approximation, following [20]. An ensemble with trajectories of the original SDE without any constraints was built. With this ensemble we perform conditioned statistics selecting those paths ending within a small neighborhood of a, that is, $A_{11}(0) \in [a - da, a + da]$ ($A_{12}(0) \in [a - da, a + da]$ if we are looking at transverse gradients). To increase the ensemble sizes, if the searched value a is crossed by any component, we perform frame rotations over the entire trajectory so that it always corresponds to component A_{11} (in the diagonal case) or A_{12} (off-diagonal). What is seen is that these paths concentrate around the instanton solution and after being averaged they tend to superpose with it as depicted in figure 4. Figure 4(a) shows several components of velocity gradients from conditionally averaged trajectories compared to the instanton solution with final value $A_{12}(0) = -0.8$. Figure 4(b) depicts how the unconditioned component $A_{22}(t)$ evolves for different final values of the conditioned $A_{12}(0)$ in comparison with instanton solution. The agreement is better as the constrained final value gets larger, as expected by instanton theory. This trend has been found in the context of Burgers equation in [20] and [21]. After all it is clearly obtained that typical trajectories of the stochastic dynamics fluctuate around but not far from the instanton trajectory provided g is small in accordance with the large deviation principle.

Conversely, the most probable trajectory leading to a certain value of longitudinal velocity gradient is such that the velocity gradient is diagonal, as claimed in section 3.2 by symmetry arguments. This statement is indeed confirmed by the filtering procedure as presented in figure 5. Figure 5(a) shows the average behaviour of velocity gradient conditioned to $A_{11}(0) = 1.0$ in comparison with instanton trajectories. All off-diagonal components vanish, as illustrated by $A_{12}(t)$ and $A_{21}(t)$ (others not shown). In figure 5(b) three different constrained values are exhibited. In contrast to the previous case the agreement does not improve for larger values of $A_{11}(0)$, another manifestation of the mismatch observed on the tails of the diagonal pdf (figure 2).
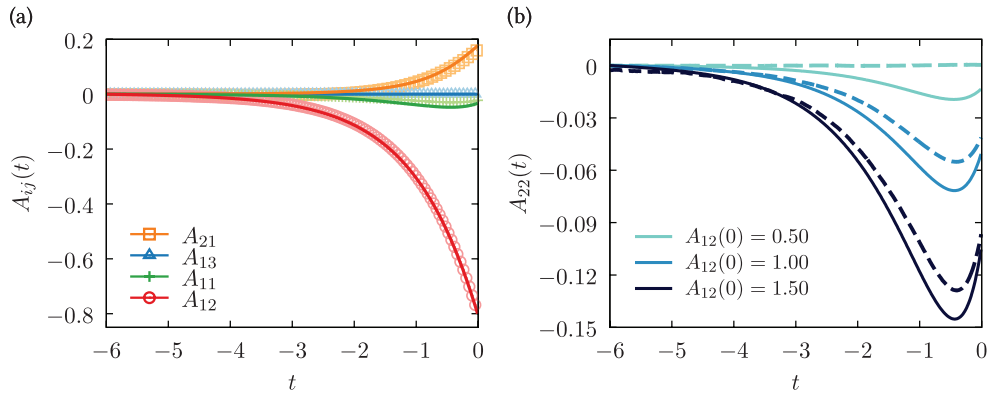
Figure 4. (a) Different components from conditionally averaged trajectories (symbols) compared to the instanton (solid) for the case where A_{12} is set to -0.8 at the endpoint. Components A_{13}, A_{23}, A_{31}, A_{32} (not all shown) are negligible, in agreement with our symmetry argument. (b) Component A_{22} both from filtering (dashed) and instanton (solid) for the case where A_{12} is set to 0.5, 1.0 and 1.5 at the endpoint. In both figures $g = 0.5$.
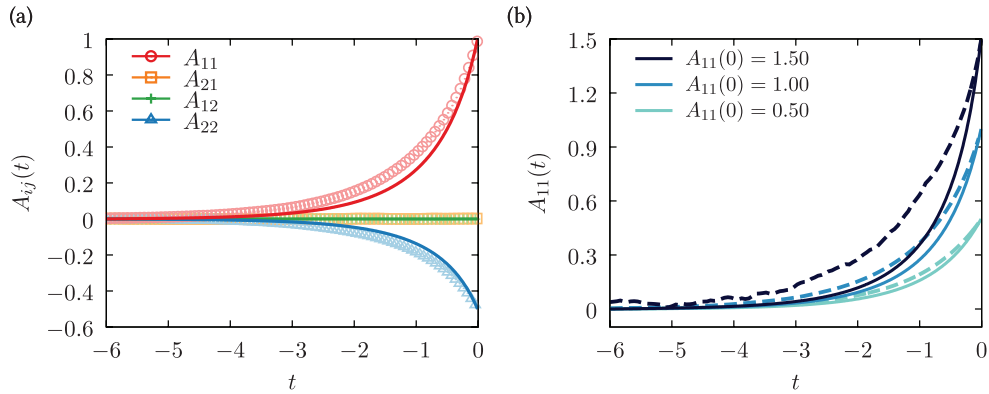

Figure 5. (a) Different components from conditionally averaged trajectories (symbols) compared to the instanton (solid) for the case where A_{11} is set to 1.0 at the endpoint. Components A_{21}, A_{12} are negligible (as well as other off-diagonal components not shown), in agreement with our symmetry argument. (b) Component A_{11} both from filtering (dashed) and instanton (solid) for the case where A_{11} is set to 0.5, 1.0 and 1.5 at the endpoint. In both figures $g = 0.5$.

4. Conclusion

The role of rare events can be revealed by means of the Martin–Siggia–Rose path integral formulation. In this work we apply this technique to a model of Lagrangian turbulence called the recent fluid deformation (RFD). This closure comprises a stochastic model of the velocity gradient based on short time correlations in the Lagrangian frame. Within the path integral formalism the most probable trajectory that leads to a certain event is calculated numerically and, for the longitudinal velocity gradient case, also analytically. We showed the use of symmetries can rule out unnecessary degrees of freedom allowing less numerical effort in order to compute the instanton. Apart from the benefited numerical computation, the symmetries

let us evaluate an analytical approximated solution for the longitudinal velocity gradient pdf, enabling us to unveil its central moments dependence on the Reynolds number.

Both longitudinal and transverse cases present the instanton satisfying the Vielleifosse line. We believe that the rationale for that lies in the dominance of the non deviatoric terms figuring the model equation (2.7). That is, when $\tau \to 0$, the RFD approximation approaches the restricted Euler equation.

Regarding vorticity alignment, instanton solutions for transverse gradients shows a complete alignment with the intermediate strain eigenvalue, which can be seen computing the normalized product of the three rate of strain eigenvalues $s^* = -3\sqrt{6}\,\lambda_1\lambda_2\lambda_3/(\lambda_1^2 + \lambda_2^2 + \lambda_3^2)^{3/2}$ [26], resulting $s^* = 1$, where $\lambda_i, i = 1, 2, 3$, are the referred eigenvalues. Since the instanton corresponds to the most probable trajectory leading to a certain value of the velocity gradient, our result agrees with [26] which showed that the pdf of s^* develops a sharp peak around $s^* = 1$.

The longitudinal velocity gradient pdf has a weaker agreement in comparison with the transverse one as the forcing increases, showing the instanton approximation is not enough to account for the full statistics even for moderately low values of g. It means that fluctuations around the instanton solution may play an essential role, which could be hopefully analyzed by perturbative methods. Perturbative corrections to the instanton pdf can be dealt with the effective action approach [8] and is currently under study. The issue of whether the instanton approach suffices and perturbative methods are fit for more complex fluid dynamical systems is an important matter and deserves further investigation.

As a final remark, the application of the instanton study to this Lagrangian model allowed us to understand the scaling of the statistical moments with the Reynolds numbers. This opens new possibilities in the direction of refinement of the RFD approximation in order to grasp more aspects of the phenomenology of turbulence. Moreover we expect that the use of symmetries as in this work, which led to a reduction of the degrees of freedom, can be applied to other stochastic systems allowing more efficient optimal path computation.

Acknowledgments

Appendix

We shall present a pedagogical derivation of the instanton boundary conditions. For this purpose it is more convenient to use the Onsager–Machlup S_{OM} action [18] rather than Martin–Siggia–Rose S_{MSR}. To change from S_{MSR} to S_{OM} one needs to integrate over the auxiliary variable $\hat{\mathbb{A}}$. For the RFD, in particular, one should notice that the tensor G_{ijkl} is not invertible, so the trace free property of the velocity gradient and the stochastic force should be taken into account. After a straightforward computation the cumulant generating function (3.1) may be rewritten as

$$\mathbb{E}[\lambda A_{\alpha\beta}(t_2)/g^2] = \int D[\mathbb{A}] \, \exp\left[-(S_{OM}[\mathbb{A}] - \lambda A_{\alpha\beta}(t_2))/g^2\right], \tag{A.1}$$

where the Onsager–Machlup action $S_{OM}[\mathbb{A}]$ reads

$$S_{\mathrm{OM}}[\mathbb{A}, \dot{\mathbb{A}}] = \frac{1}{2} \int_{t_1}^{t_2} \mathrm{d}t \left[(\dot{A}_{ij} - V_{ij}) Q_{ijkl}^{-1} (\dot{A}_{kl} - V_{kl}) - \frac{1}{5} \mathrm{Tr}[\dot{\mathbb{A}} - \mathbb{V}]^2 \right], \quad \text{(A.2)}$$

with $Q_{ijkl}^{-1} = (8/15)\delta_{ik}\delta_{jl} + (-2/15)\delta_{il}\delta_{jk}$ such that $G_{ijkl} = Q_{ijkl} - Q_{ijmm} \, Q_{klnn} \, /Q_{ppqq}$.

The specific form of the Onsager–Machlup Lagrangian is not important for the general derivation below. We calculate the action variation with respect to the path $\mathbb{A}(t)$ with initial point fixed, that is, $\delta\mathbb{A}(t_1) = 0$, yielding

$$
\begin{aligned}
\delta S &= \int_{t_1}^{t_2} \mathrm{d}t \left\{ \mathrm{Tr}\left[\frac{\partial \mathcal{L}}{\partial \mathbb{A}} \delta\mathbb{A}^T(t) + \frac{\partial \mathcal{L}}{\partial \dot{\mathbb{A}}} \delta\dot{\mathbb{A}}^T(t) \right] + \lambda\delta(t - t_2)\,\delta A_{\alpha\beta}(t) \right\} \\
&= \int_{t_1}^{t_2} \mathrm{d}t \, \mathrm{Tr}\left[\frac{\partial \mathcal{L}}{\partial \mathbb{A}} \delta\mathbb{A}^T(t) + \frac{\mathrm{d}}{\mathrm{d}t}\left(\frac{\partial \mathcal{L}}{\partial \dot{\mathbb{A}}} \delta\mathbb{A}^T(t) \right) - \frac{\mathrm{d}}{\mathrm{d}t}\frac{\partial \mathcal{L}}{\partial \dot{\mathbb{A}}} \delta\mathbb{A}^T(t) \right] \\
&\quad + \lim_{\epsilon \to 0} \int_{t_1}^{t_2+\epsilon} \mathrm{d}t \, \lambda\,\delta(t - t_2)\,\delta A_{\alpha\beta}(t) \\
&= \int_{t_1}^{t_2} \mathrm{d}t \, \mathrm{Tr}\left[\left(\frac{\partial \mathcal{L}}{\partial \mathbb{A}} - \frac{\mathrm{d}}{\mathrm{d}t}\frac{\partial \mathcal{L}}{\partial \dot{\mathbb{A}}} \right)\delta\mathbb{A}^T(t) \right] + \mathrm{Tr}\left(\frac{\partial \mathcal{L}}{\partial \dot{\mathbb{A}}} \delta\mathbb{A}^T(t) \right)_{t_1}^{t_2} + \lambda\,\delta A_{\alpha\beta}(t_2) \quad \text{(A.3)}
\end{aligned}
$$

By demanding the action variation to be stationary with respect to the path $\mathbb{A}(t)$ we arrive at

$$\frac{\partial \mathcal{L}}{\partial \mathbb{A}} - \frac{\mathrm{d}}{\mathrm{d}t}\frac{\partial \mathcal{L}}{\partial \dot{\mathbb{A}}} = 0 \quad \text{(A.4)}$$

$$\mathrm{Tr}[\mathbb{P}(t_2)\,\delta\mathbb{A}^T(t_2)] - \mathrm{Tr}[\mathbb{P}(t_1)\,\underbrace{\delta\mathbb{A}^T(t_1)}_{=0}] + \lambda\,\delta A_{\alpha\beta}(t_2) = 0, \quad \text{(A.5)}$$

where we used the conjugated momentum $\mathbb{P}(t) = \partial\mathcal{L}/\partial\dot{\mathbb{A}}(t)$ in the last equality. Equation (A.4) is the Euler–Lagrange equation which gives the evolution with time, while (A.5) implies the final condition for the conjugated momenta $P_{ij}(t_2) = -\delta_{i\alpha}\delta_{j\beta}\lambda$. The second term in equation (A.5) vanishes owing to the initial condition set to $\mathbb{A}(t_1)$, where no variation is allowed.

References

[1] Chevillard L and Meneveau C 2006 *Phys. Rev. Lett.* **97** 174501
[2] Chernykh A I and Stepanov M G 2001 *Phys. Rev.* E **64** 026306
[3] Sreenivasan K R and Antonia R A 1997 *Annu. Rev. Fluid Mech.* **29** 435
[4] Afonso M M and Meneveau C 2010 *Physica* D **239** 1241
[5] Chevillard L and Meneveau C 2011 *Phys. Fluids* **23** 101704
[6] Chevillard L, Meneveau C, Biferale L and Toschi F 2008 *Phys. Fluids* **20** 101504
[7] Hater T, Homann H and Grauer R 2011 *Phys. Rev.* E **83** 017302
[8] Moriconi L, Pereira R M and Grigorio L S 2014 *J. Stat. Mech.* P10015
[9] Meneveau C 2011 *Ann. Rev. Fluid Mech.* **43** 219
[10] Freidlin M I and Wentzell A D 2012 *Random Perturbations of Dynamical Systems* (Berlin: Springer)
[11] Touchette H 2009 *Phys. Rep.* **478** 1
[12] Vieillefosse P 1984 *Physica* A **125** 150
[13] Cantwell B J 1992 *Phys. Fluids* A **4** 782
[14] Chertkov M, Pumir A and Shraiman B I 1999 *Phys. Fluids* **11** 2394
[15] Martin P C, Siggia E D and Rose H A 1973 *Phys. Rev.* A **8** 423
[16] Janssen H K 1976 *Z. Phys.* B: Cond. Mat. **23** 377
[17] De Dominicis C 1976 *J. Physique Colloque* **37** 247

[18] Onsager L and Machlup S 1953 *Phys. Rev.* **91** 1505
[19] Guraire V and Migdal A C 1996 *Phys. Rev.* E **54** 4908
[20] Grafke T, Grauer R and Schäfer T 2013 *J. Phys. A: Math. Theor.* **46** 62002
[21] Grafke T, Grauer R, Schäfer T and Vanden-Eijnden E 2015 *Eurphys. Lett.* **109** 34003
[22] Grafke T, Grauer R and Schäfer T 2015 *J. Phys. A: Math. Theor.* **48** 333001
[23] Bouchet F, Laurie J and Zaboronski O 2014 *J. Stat. Phys.* **156** 1066–92
[24] Kloeden P E and Platen E 1999 *Numerical Solution of Stochastic Differential Equations* (Berlin: Springer)
[25] Chevillard L and Meneveau C 2007 *C. R. Mec.* **335** 187
[26] Lund T and Rogers M 1994 *Phys. Fluids* **6** 1838